2007

Computational enhancement of large scale environmental imagery: aggregation of robust numerical regularization, neural computing and digital dynamic filtering

Shkvarko, Yuriy; Villalón-Turrubiates, Iván E.

Y. Shkvarko & I.E. Villalón-Turrubiates (2007). “Computational enhancement of large scale environmental imagery: aggregation of robust numerical regularization, neural computing and digital dynamic filtering”, International Journal of Computational Science and Engineering (IJCSE), 3(3), pp.219-231.

Computational enhancement of large scale environmental imagery: aggregation of robust numerical regularisation, neural computing and digital dynamic filtering

Yuriy Shkvarko* and Ivan Villalon

Department of Telecommunications,
CINVESTAV Campus Guadalajara,
Av. Científica 1145, Col. El Bajio,
Guadalajara, Jalisco C.P. 45015, Mexico
E-mail: shkvarko@gdl.cinvestav.mx E-mail: villalon@gdl.cinvestav.mx
*Corresponding author

Abstract: We address a new efficient robust optimisation approach to large-scale environmental image reconstruction/enhancement as required for remote sensing imaging with multi-spectral array sensors/SAR. First, the problem-oriented robustification of the previously proposed Fused Bayesian-Regularization (FBR) enhanced imaging method is performed to alleviate its ill-poseness due to system-level and model-model uncertainties. Second, the modification of the Hopfield-type Maximum Entropy Neural Network (MENN) is proposed that enables such MENN to perform numerically the robustified FBR technique via computationally efficient iterative scheme. The efficiency of the aggregated robust regularised MENN technique is verified through simulation studies of enhancement of the real-world environmental images.

Keywords: nonlinear regularisation; image enhancement; numerical inverse problems; entropy; neural networks.

Reference to this paper should be made as follows: Shkvarko, Y. and Villalon, I. (2007) 'Computational enhancement of large scale environmental imagery: aggregation of robust numerical regularisation, neural computing and digital dynamic filtering', *Int. J. Computational Science and Engineering*, Vol. 3, No. 3, pp.219–231.

Biographical notes: Y. Shkvarko, Eng. (Hon.) 1976, PhD 1980, DSc 1990. From 1976 to 1991, was with the Scientific Research Department of the Kharkov Aviation Institute, Kharkov, ex USSR, From 1991 to 1999, and a Professor at the Ukrainian National Polytechnic Institute at Kharkov, Ukraine. From 1999 to 2001, he was a visiting professor in the Guanajuato State University at Salamanca, Mexico. In 2001, he joined the CINVESTAV-Guadalajara (Centre for Advanced Research and Studies) of Mexico as a Titular Professor. His research interests are in applications of signal processing to remote sensing, imaging radar, navigation and communications.

I. Villalon, Mechanical Engineer (2000), Master in Sciences in Electrical Engineering (2003), Doctor in Sciences in Electrical Engineering (2007). Presently, he is with the Department of Computer Sciences and Engineering of the University of Guadalajara in Mexico as a Full-time Professor/Researcher. His research work is in applications of signal and image processing to remote sensing. He has published 19 papers in international journals and conference proceedings and 2 chapters in a book on these topics.

1 Introduction

Numerical reconstructive image processing is now a mature and well developed research field, presented and detailed in many works, (see all the references). Although the existing theory offers a manifold of statistical and descriptive regularisation techniques for reconstructive imaging in many application areas there still remain some unresolved crucial theoretical-level and computational-level problems related to large scale sensor array or synthesised array real-time reconstructive image processing. In this study, as a particular application area, we consider the reconstructive Remote Sensing (RS) imaging with the use of array sensor systems, e.g., array radars (Haykin and Steinhardt, 1992; Shkvarko, 2002a, 2002b) or Synthetic Aperture Radars (SAR) (Henderson and Lewis, 1998; Mahafza, 2000). The particular problems that we are going to detail and treat in this paper relate to substantial reduction of the computational load of the recently developed optimal/suboptimal nonlinear Bayesian/regularisation image reconstruction procedures (Astola and Kuosmanen, 1997; Haykin and Steinhardt, 1992; Henderson and

Lewis, 1998, Shkvarko, 2002a, 2002b, 2004a, 2004b; Starck et al., 1998) via performing their robustification aggregated with efficient real-time numerical implementation that employs the Neural Network (NN) computing. Three principal algorithmic-level and NN computational-level developments constitute major innovative contributions of this study, namely:

1.1 First stage: Robustification of the FBR method

At this level of study, we develop the robustified numerical version of the Fused Bayesian-Regularization (FBR) method (Shkvarko, 2002a, 2002b, 2004a, 2004b) for reconstruction of the power Spatial Spectrum Pattern (SSP) of the wave field scattered from the remotely sensing scene (that is referred to as a desired RS image (Shkvarko, 2002a, 2002b) given a finite set of array radar/SAR signal recordings. Since this is in essence a nonlinear numerical inverse problem, we propose to alleviate the problem illposeness by robustification of the Bayesian estimation strategy (Shkvarko, 2002a, 2002b; Starck et al., 1998; Stoica and Moses, 1997) via performing the non adaptive approximations of the reconstructive operators that incorporate the non-trivial metrics considerations for designing the proper solution space and differerent regularisation constraints imposed on a solution. Pursuing such an approach we develop the family of robustified versions of the FBR method of different computational complexity that we address as the robustified real-time RS image reconstruction algorithms.

1.2 Second stage: Modification of NN computing scheme

Here, we derive a numerical technique for efficient real-time computational implementation of the robustified RS image reconstruction/enhancement algorithms that employ the NN computing paradigm. In particular, we propose to employ the general Li's architecture of the Hopfield-type dynamic NN detailed by Shkvarko (2001) but modify the specifications of the NN's parameters (i.e., synaptic weights and bias inputs in all the NN's loops, as well as the NN's state update rule) to enable such the modified NN to perform the real-time robust image reconstruction/enhancement tasks. The new proposed method is addressed to as the aggregated robust regularised MENN (ARRMENN) technique.

1.3 Third stage: Towards dynamic computing

The last issue that we address as a perspective innovation is an idea of incorporating the concept of dynamic computing into the ARRMENN technique to enable the latter to reconstruct the desired environmental imagery taking into account dynamical behaviour of particular Remote Sensing Signatures (RSS). This provides a background for understanding the future trends in development of intelligent dynamic RS imaging and resource management techniques.

2 Problem formalism

2.1 RS-motivated problem model

The generalised mathematical formulation of the problem considered in the present study is similar in notation and structure to that by Shkvarko (2002a, 2002b, 2004a, 2004b), and some crucial elements are repeated for convenience to the reader. Consider a remote sensing experiment performed with a coherent array imaging radar or SAR (radar/SAR) that is traditionally referred to as Radar Imaging (RI) problem (Henderson and Lewis, 1998; Shkvarko, 2002a, 2002b, 2004a, 2004b). The measurement sensor/SAR data wavefield $u(\mathbf{y}) = s(\mathbf{y}) + n(\mathbf{y})$ modelled as a superposition of the echo signals s and additive noise n and is assumed to be available for observations and recordings within the prescribed time-space observation domain $Y \ni \mathbf{y}$, where $\mathbf{y} = (t, \mathbf{p})^T$ defines the time-space points in the observation domain $Y = T \times P$. The model of the observation wavefield u is specified by the linear stochastic Equation of Observation (EO) of operator form (Shkvarko, 2002a, 2002b):

$$u = Se + n; \quad e \in E; \quad u, n \in U; \quad S: E \to U \tag{1}$$

on the Hilbert signal spaces E and U with the metric structures induced by the inner products,

$$\begin{aligned} \left[e_1, e_2\right]_{\mathbf{E}} &= \int_X e_1(\mathbf{x}) e_2^*(\mathbf{x}) \mathrm{d}\mathbf{x} \quad \text{and} \\ \left[e_1, e_2\right]_{\mathbf{U}} &= \int_Y u_1(\mathbf{y}) u_2^*(\mathbf{y}) \mathrm{d}\mathbf{y}, \end{aligned} \tag{2}$$

respectively, where asterisk stands for complex conjugate. In the EO (1), the S is referred to as the regular Signal Formation Operator (SFO). It defines the transform of random scattered signals $e(\mathbf{x}) \in \mathrm{E}(X)$ distributed over the remotely sensed scene (probing surface) $X \ni \mathbf{x}$ into the echo signals $(Se(\mathbf{x}))(\mathbf{y}) \in \mathrm{U}(Y)$ over the time-space observation domain $Y = T \times P$; $t \in T$, $\mathbf{p} \in P$. In the functional terms (Shkvarko, 2002a, 2002b; Starck et al., 1998), such a transform is referred to as the operator $S : \mathrm{E} \to \mathrm{U}$ that maps the scene signal space E (the space of the signals scattered from the remotely sensed scene) onto the observation data signal space U. The operator model of the stochastic EO (1) in the conventional integral form (Shkvarko, 2002a, 2002b) may be rewritten as

$$u(\mathbf{y}) = \int_X S(\mathbf{y}, \mathbf{x}) e(\mathbf{x}) d(\mathbf{x}) + n(\mathbf{y}), \tag{3}$$

$$e(\mathbf{x}) = e(f; \boldsymbol{\rho}, \boldsymbol{\theta}) = \int_F e(t, \boldsymbol{\rho}, \boldsymbol{\theta}) \exp(-j2\pi ft) dt \tag{4}$$

where the functional kernel $S(\mathbf{y}, \mathbf{x})$ of the SFO S given by equation (1) defines the signal wavefield formation model (Mahafza, 2000). Following the multi-scale array/SAR radar RS problem phenomenology (Henderson and Lewis, 1998; Shkvarko, 2002a, 2002b) we assume an incoherent nature of the backscattered field $e(\mathbf{x})$ over the frequency-space observation domain $X = F \times R = F \times P \times \Theta$; in the

slant range $\boldsymbol{\rho} \in P$ and azimuth angle $\boldsymbol{\theta} \in \Theta$ domains, respectively. When tackling the RS spatial analysis problems, the radar engineers typically work in the frequency-space domain, $\mathbf{x} = (f, \boldsymbol{\rho}, \boldsymbol{\theta})^T \in X = F \times P \times \Theta$ (Henderson and Lewis, 1998; Mahafza, 2000; Shkvarko, 2002a, 2002b). However, because of the one-to-one mapping, only the spatial cross range coordinates $\mathbf{r} = (\boldsymbol{\rho}, \boldsymbol{\theta})$ may be associated with $\mathbf{x}$ as well (Mahafza, 2000). Such interpretation is valid if one assumes the narrowband system model (Doerry et al., 2002) and incoherent nature of the backscattered field $e(\mathbf{x})$ (Mahafza, 2000).

This is naturally inherent to the RS imaging experiments (Mahafza, 2000; Shkvarko, 2004a, 2004b) in which case the phasor $e(f, \mathbf{r})$ in equation (4) is taken to be independent random variable at each frequency f, and spatial coordinates $\mathbf{r}$, θ with the zero mean value and δ-form correlation function, $R_E(f, f'; \mathbf{r}, \mathbf{r}') = < E(f, \mathbf{r}^*) E^*(f', \mathbf{r}') > = B(f, \mathbf{r})\, \delta(f - f')\delta(\mathbf{r} - \mathbf{r}')$ that enables one to introduce the following definition of the Spatial Spectrum Pattern (SSP) of the wavefield sources distributed in the observation environment (Doerry et al., 2002)

$$B(r) = Aver^{(2)}\{e(\mathrm{r})\} = \int_F < e(f, \mathbf{r}) e^*(f, \mathbf{r} > |\, H(f)\,|^2\, df; \quad \mathbf{r} \in \mathrm{R} : \boldsymbol{\rho} \in P; \boldsymbol{\theta} \in \Theta. \tag{5}$$

Here, <·> represents the ensemble averaging operator, while $Aver^{(2)}$ is referred to as the second order (i.e., nonlinear) statistical averaging operator defined by equation (5). Also in equation (5), $H(f)$ represents the given transfer function of the radar receiving channels that we assume to be identical for all antenna array elements and impose the conventional normalisation, $|H(f)|^2 = 1$ for all frequencies $f \in F$ in the radar receiver frequency integrating band F (Puetter, 1996).

Following the described by Haykin and Steinhardt (1992) and by Shkvarko (2002a, 2002b), the initial RS imaging problem is stated as estimation $\hat{B}(\mathbf{x})$ of the SSP $B(\mathbf{r})$ over the remotely sensed scene $R \ni \mathbf{r}$ by processing whatever values of measurements of the data $u(\mathbf{y})$; $\mathbf{y} \in Y$, are available. Next, following the RS methodology described by Shkvarko (2002a, 2002b), any particular physical signature of interest $\hat{\Lambda}(\mathbf{x})$ could be extracted from the reconstructed RS image $\hat{B}(\mathbf{x})$ applying the so-cold deterministic signature extraction operator Λ. Hence, the particular RSS is mapped applying Ëto the reconstructed image, i.e.,

$$\hat{\Lambda}(\mathbf{x}) = \Lambda(\hat{B}(\mathbf{x})). \tag{6}$$

Last, taking into account the RSS extraction model (6), we can reformulate now the signature reconstruction problem as follows: to map the reconstructed particular RSS of interest $\hat{\Lambda}(\mathbf{x}) = \Lambda(\hat{B}(\mathbf{x}))$ over the observation scene $X \ni \mathbf{x}$ by post-processing whatever values of the reconstructed scene image $\hat{B}(\mathbf{x})$; $\mathbf{x} \ni X$, are available.

2.2 Projection-based numerical model of the problem

Viewing it as an approximation problem leads one to the projection concept for a transformation of the continuous data field $u(\mathbf{y})$ to the $M \times 1$ vector $\mathbf{U} = (U_1, \ldots, U_M)^T$ of sampled spatial-temporal data recordings. The M-d observations in the terms of projections (Shkvarko, 2004a, 2004b) can be expressed as

$$u_{(M)}(\mathbf{y}) = P_{U(M)} u(\mathbf{y}) = \sum\nolimits_{m=1}^{M} U_m \phi_m(\mathbf{y}) \tag{7}$$

with coefficients $U_m = [u, h_m]_U$ where $P_U(M)$ represents a projector onto the M-d observation subspace (Astola and Kuosmanen, 1997)

$$U_{(M)} = P_{U(M)} U = Span\{\phi_m(\mathbf{y})\} \tag{8}$$

uniquely defined by a set of the orthogonal functions $\{\phi_m(\mathbf{y}) = \|h_m(\mathbf{y})\|^{-2} h_m(\mathbf{y});\ m = 1, \ldots, M\}$ that are related to $\{h_m(\mathbf{y})\}$ as a dual basis in $U(M)$ i.e., $[h_m, \phi_n]_U = \delta_{mn}\ \forall\ m, n = 1, \ldots, M$.

In the observation scene $X \ni \mathbf{x}$, the discretisation of the scattering field $e(\mathbf{x})$ is traditionally performed over a $Q \times N$ rectangular grid where Q defines the dimension of the grid over the horizontal (azimuth) coordinate x_1 and N defines the grid dimension over the orthogonal coordinate x_2 (the number of the range gates projected onto the scene). The discretised complex scattering function is represented by coefficients (Shkvarko, 2004a, 2004b) $E_k = \mathrm{E}_{(q,n)} = [e, g_k]_E = \int e(\mathbf{x}) g_k(\mathbf{x}) \mathrm{d}\mathbf{x}$; $k = 1, \ldots, K = Q \times N$, of it decomposition over the grid composed of such identical shifted rectangular functions $\{g_k(\mathbf{x}) = g_{(q,n)}(\mathbf{x}) = 1$ if $\mathbf{x} \in \rho_{(q,n)}(\mathbf{x}) = \mathrm{rect}_{(q,n)}(x_1, x_2)$ and $g_k(\mathbf{x}) = 0$ for other $\mathbf{x} \notin \rho_{(q,n)}(\mathbf{x})$ for all $q = 1, \ldots, Q$; $n = 1, \ldots, N$; $k = 1, \ldots, K = Q \times N\}$. Hence, the K-d approximation of the scattering field becomes

$$e_{(K)}(\mathbf{x}) = (\mathrm{P}_{E(K)} e)(\mathbf{x}) = \sum_{k=1}^{K} E_k g_k(\mathbf{x}) \tag{9}$$

where $P_{E(K)}$ represents a projector onto the K-d signal approximation subspace

$$E_K = P_{E(K)} E = \mathrm{Span}\{g_k(\mathbf{x})\} \tag{10}$$

spanned by K orthogonal grid functions (pixels) $\{g_k(\mathbf{x})\}$.

Using such approximations, we proceed from the operator form EO (1) to its conventional numerical (vector) form

$$\mathbf{U} = \mathbf{S}\mathbf{E} + \mathbf{N}, \tag{11}$$

where $\mathbf{U}$, $\mathbf{N}$ and $\mathbf{E}$ define the vectors composed of the coefficients U_m, N_m and E_k of the finite-dimensional approximations of the fields u, n and e, respectively, and $\mathbf{S}$ is the matrix-form representation of the SFO with elements $\{S_{mk} = [Sg_k, h_m]_U = \int (Sg_k(\mathbf{x}))(\mathbf{y}) h_m^*(\mathbf{y}) d\mathbf{y};$ $k = 1, \ldots, K; m = 1, \ldots, M\}$ (Shkvarko, 2002a, 2002b).

Zero-mean Gaussian vectors **E**, **N** and **U** in equation (11) are characterised by the correlation matrices, $\mathbf{R_E}$, $\mathbf{R_N}$ and $\mathbf{R_U} = \mathbf{SR_E S}^{+} + \mathbf{R_N}$, respectively, where superscript $+$ defines the Hermitian conjugate when it stands with a matrix. Because of the incoherent nature of the scattering field $e(\mathbf{x})$, the vector **E** has a diagonal correlation matrix, $\mathbf{R_E} = \mathrm{diag}\{\mathbf{B}\} = \mathbf{D(B)}$, in which the $K \times 1$ vector of the principal diagonal **B** is composed of elements $B_k = < E_k E_k^{*} >; k = 1,\ldots,K$. This vector **B** is referred to as a vector-form representation of the SSP, i.e., the SSP vector defined by Shkvarko (2002a, 2002b, 2004a, 2004b). Hence, using the model (6) the K-d approximation of the desired RS signature estimate $\hat{\Lambda}_{(K)}(\mathbf{x})$ as a continuous function of $\mathbf{x} \in X$ over the probing scene X is now expressed as follows

$$\hat{\Lambda}_{(K)}(\mathbf{x}) = est\left\{\Lambda < \mid e_{(K)}(\mathbf{x}) \mid^2 >\right\} = \sum_{k=1}^{K} \Lambda(\hat{B}_k) g_k(\mathbf{x}); \mathbf{x} \in X\Big\}. \tag{12}$$

Analysing equation (12), one may deduce that in every particular measurement scenario (specified by the corresponding approximation spaces $\mathrm{U}_{(M)}$ and $\mathrm{E}_{(K)}$) one has to derive the estimate $\hat{\mathbf{B}}$ of a vector-form approximation of the SSP that uniquely defines via equation (12) the approximated continuous reconstructed map $\hat{\Lambda}_{(K)}(\mathbf{x})$ of the desired RS signature distributed over the observed scene $X \ni \mathbf{x}$. Hence, the vector

$$\hat{\Lambda} = vec\left\{\Lambda(\hat{B}_k); k = 1,\ldots,K\right\} \tag{13}$$

represents the numerical (vector-form) model of the reconstructed RS signature in the conventional pixel format. The latter is uniquely reconstructed from the original RS image $\hat{\mathbf{B}}$. Thus, we may restrict our further study to reconstruction of the SSP vector $\hat{\mathbf{B}}$ that uniquely determines through equation (13) the resulting pixel-format map of the desired RS signature.

2.3 Experiment Design(ED) considerations

The Experiment Design (ED) aspects of this problem involving the analysis of how to choose (finely adjust) the basis functions $\{g_k(\mathbf{r})\}$ that span the signal representation subspace $\mathrm{E}_{(K)} = P_{E(K)}\mathrm{E} = \mathrm{Span}\{g_k\}$ for a given observation subspace $\mathrm{U}_{(M)} = \mathrm{Span}\{\varphi_m\}$ were investigated in more details by Shkvarko (2002a, 2002b, 2004a, 2004b). Also, we employ here the ED considerations regarding the metrics structure in the solution space defined by the inner product (Shkvarko, 2004a, 2004b)

$$\| \mathbf{B} \|^2_{B(K)} = [\mathbf{B}, \mathbf{MB}] \tag{14}$$

where **M** is referred to as the metrics inducing operator. Hence, the selection of **M** provides the additional geometrical degrees of freedom of the problem model. In this paper, we incorporate the model of **M** that corresponds to the numerical approximation of the Tikhonov's stabiliser of the second order that was numerically designed by Shkvarko (2004a, 2004b). Also, following the work of Shkvarko (2004a, 2004b), we incorporate the projection-type a priori information requiring, the SSP vector **B** satisfies the linear constraint equation

$$\mathbf{GB} = \mathbf{C}, \textit{i.e.}, \mathbf{G}^{-}\mathbf{GB} = \mathbf{B}_P \tag{15}$$

where $\mathbf{B}_P = \mathbf{G}\,\mathbf{C}$ and $\mathbf{G}^{-}$ is the Moore-Penrose (Mesarovic et al., 1995) pseudoinverse of a given projection operator **G**: $\mathrm{B}_{(K)} \to \mathrm{B}_{(Q)}$, and the constraint vector $\mathbf{C} \in \mathbf{B}_{(Q)}$ and the constraint subspace $\mathrm{B}_{(Q)}$ ($Q < K$) are assumed to be given. In equation (15), the constraint operator **G** projects the portion of the unknown SSP onto the subspace where the SSP values are fixed by **C**. In practice, such limitations may specify the system calibration (Bell and Narayanan, 2001). The main purpose of this paper is to present the efficient real-time implementation techniques for the robustified (suboptimal) versions of the FBR optimal estimator derived previously by Shkvarko (2002a, 2002b, 2004a, 2004b) via performing the relevant array data processing. Thus we limit our study here to the implementation aspects of the SSP estimation problem via performing the robustification of the FBR method (Shkvarko, 2002a, 2002b, 2004a, 2004b) for the generalised model (3) of the SSP of the wavefield sources collected (integrated) over the prescribed frequency observation band. Such a generalisation distinguishes the present study from the frequency independent SSP estimation that was considered by Shkvarko (2002a, 2002b, 2004a, 2004b).

3 FBR method

The estimator that produces the optimal estimate $\hat{\mathbf{B}}$ of the SSP vector via processing the M-D data recordings **U** applying the FBR estimation strategy that incorporates nontrivial a priori geometrical and projection-type model information was developed in our previous study (Shkvarko, 2004a, 2004b). Such optimal FBR estimate of the SSP is given by the nonlinear equation (Shkvarko, 2004a, 2004b) that we generalise here for the case of the integrated SSP model as follows

$$\hat{\mathbf{B}} = \mathbf{B}_p + \mathbf{PB}_0 + \mathbf{W}(\hat{\mathbf{B}})\{\mathbf{V}(\hat{\mathbf{B}}) - \mathbf{Z}(\hat{\mathbf{B}})\}. \tag{16}$$

In equation (16), $\mathbf{B}_P$ is defined by equation (15) and $\mathbf{B}_0$ represents the a priori SSP distribution to be considered as a zero step approximation to the desires SSP $\hat{\mathbf{B}}$. Note that in this paper, we use all the notations used by Shkvarko (2004a, 2004b) for definitions of the sufficient statistics (SS) vector $\mathbf{V}(\hat{\mathbf{B}}) = \{\mathbf{F}(\hat{\mathbf{B}})\mathbf{U}\mathbf{U}^{+}\mathbf{F}^{+}(\hat{\mathbf{B}})\}_{diag}(\{.\}_{diag}$ determines a vector composed of the principal diagonal of the embraced matrix), the solution-dependent SS formation operator

$$\mathbf{F} = \mathbf{F}(\hat{\mathbf{B}}) = \mathbf{D}(\hat{\mathbf{B}})(\mathbf{I} + \mathbf{S}^{+}\mathbf{R}_{\mathbf{N}}^{-1}\mathbf{S}\mathbf{D}(\hat{\mathbf{B}}))^{-1}\mathbf{S}^{+}\mathbf{R}_{\mathbf{N}}^{-1}, \quad (17)$$

the SS shift vector $\mathbf{Z}(\hat{\mathbf{B}})$ (Shkvarko, 2004a, 2004b), and the composite solution-dependent smoothing-projection window operator (Shkvarko, 2004a, 2004b)

$$\mathbf{W}(\hat{\mathbf{B}}) = \mathbf{P}_{\mathbf{W}}\mathbf{\Omega}(\hat{\mathbf{B}}) \quad (18)$$

with the projector

$$\mathbf{P}_{\mathbf{W}} = (\mathbf{I} - \mathbf{G}^{-}\mathbf{G}) \quad (19)$$

and solution dependent smoothing window

$$\mathbf{\Omega}(\hat{\mathbf{B}}) = (diag\{\{\mathbf{S}^{+}\mathbf{F}^{+}\mathbf{F}\mathbf{S}\}_{diag}\} + \hat{\alpha}\mathbf{D}^{2}(\hat{\mathbf{B}})\mathbf{M}(\hat{\mathbf{B}}))^{-1} \quad (20)$$

in which the regularisation parameter $\hat{\alpha}$ is to be adaptively adjusted using the system calibration data (Shkvarko, 2004a, 2004b).

Next, applying the signature extraction model defined by equation (13) we get the final FBR-optimal estimate of the desired RSS in the numerical (discrete pixel) format

$$\hat{\Lambda} = \Lambda(\hat{\mathbf{B}}) = \Lambda(\mathbf{B}_{P} + \mathbf{P}\mathbf{B}_{0} + \mathbf{W}(\hat{\mathbf{B}})\{\mathbf{V}(\hat{\mathbf{B}}) - \mathbf{Z}(\hat{\mathbf{B}})\}). \quad (21)$$

As it is obvious from the nonlinearity of equations (16), (21), because of the complexity of the solution dependent K-D operator inversions needed to be performed to compute the SS $\mathbf{V}(\hat{\mathbf{B}})$, the window $\mathbf{W}(\hat{\mathbf{B}})$ and SS shift $\mathbf{Z}(\hat{\mathbf{B}})$, the computational load of the original optimal FBR estimator (16), (21) is extremely high to address that as a practically realisable estimator of the SSP and RS signatures (i.e., practical highresolution RS radar imaging and signature mapping technique realisable to operate in a real-time mode).

4 Robust FBR-based techniques

4.1 FBR-robustified estimators

In this subsection, we propose the robustification scheme for real-time implementation of the FBR estimator (16), (21) that enables one to reduce drastically the computation load of the image formation procedure without substantial degradation in the resolution and overall image performances. We propose the robustified version of the FBR estimator (referred to as Robust Reconstructive Filtering (RRF) method) via roughing $\mathbf{P}_{\mathbf{W}} = \mathbf{I}$ and performing the robustification (nonadaptive approximation) of both the SS formation operator $\mathbf{F}(\hat{\mathbf{B}})$ and the smoothing window $\Omega(\hat{\mathbf{B}})$ in (16) by roughing $\mathbf{D}(\hat{\mathbf{B}}) \approx \mathbf{D} = \beta\mathbf{I}$, where β represents the expected a priori image grey level (Shkvarko, 2004a, 2004b). Hence, the robustified SS formation operator

$$\mathbf{F} = \mathbf{A}^{-1}(\rho)\mathbf{S}^{+} \text{ with } \mathbf{A}(\rho) = \mathbf{S}^{+}\mathbf{S} + \rho^{-1}\mathbf{I} \quad (22)$$

becomes the regularised inverse of the SFO $\mathbf{S}$ with regularisation parameter ρ^{-1}, the inverse of the Signal-to-Noise Ratio (SNR) $\rho = \beta/N_0$ for the adopted white noise model, $\mathbf{R}_{\mathbf{N}} = N_0\mathbf{I}$. The robust smoothing window

$$\mathbf{W} = \mathbf{\Omega} = (w_0\mathbf{I} + \mathbf{M})^{-1} \quad (23)$$

is completely defined now by the matrix $\mathbf{M}$ that induces the metrics structure in the solution space (Shkvarko et al., 2001) with the scaling factor $w_0 = \mathrm{tr}\{\mathbf{S}^{+}\mathbf{F}^{+}\mathbf{F}\mathbf{S}\}/K$. Note that such robustified $\mathbf{W}$ can be pre-computed a priori for a family of different admissible ρ as it was performed in the previous study (Shkvarko, 2004a, 2004b). Here, we adopt practical constraints of high SNR operational conditions (Bell and Narayanan, 2001), $\rho >> 1$, in which case one can neglect also the constant bias $\mathbf{Z} = Z_0\mathbf{I}$ in equation (16) because it does not affect the pattern of the SSP estimate (it influences only the constant gray level in the resulting solution but $Z_0 << \beta$ for $\rho >> 1$). Following these practically motivated assumptions, the resulting RRF estimators for the SSP and RSS become

$$\hat{\mathbf{B}}_{RRF} = \mathbf{B}_{0} + \mathbf{\Omega}\mathbf{V}, \quad \hat{\Lambda}_{RRF} = \Lambda(\mathbf{B}_{0} + \mathbf{\Omega}\mathbf{V}) \quad (24)$$

correspondingly, where $\mathbf{V} = \{\mathbf{F}\mathbf{U}\mathbf{U}^{+}\mathbf{F}^{+}\}_{diag}$ represents now the robust (solution independent) SS vector. Thus, the principal computational load of the RRF estimator (24) is associated now with the operator inversions required to compute the solution operator (17) for adaptively (recurrently) adjusted regularisation parameter ρ.

4.2 Robust matched spatial filtering algorithm

The simplest rough SSP and RSS estimators can be constructed as further simplification of equation (24) if we adopt the trivial a priori model information ($\mathbf{P}_{\mathbf{W}} = \mathbf{I}$ and $\mathbf{B}_0 = 0\mathbf{I}$) and roughly approximate the SS formation operator $\mathbf{F}$ by the adjoint SFO, i.e.,

$$\mathbf{F} \approx \gamma_0\mathbf{S}^{+} \quad (25)$$

where the normalising constant γ_0 provides balance of the operator norms $\gamma_0^2 = \mathrm{tr}^{-1}\{\mathbf{S}^{+}\mathbf{S}\mathbf{S}^{+}\mathbf{S}\}\ \mathrm{tr}\{\mathbf{F}\mathbf{S}\mathbf{S}^{+}\mathbf{F}^{+}\}$ (Bell and Narayanan, 2001). In that case, the estimators (24) are simplified to their rough versions

$$\hat{\mathbf{B}}_{MF} = \mathbf{\Omega}\mathbf{H}, \quad \hat{\Lambda}_{MF} = \Lambda(\mathbf{\Omega}\mathbf{H}) \quad (26)$$

respectively, where the rough SS, $\prod = \gamma_0^2\{\mathbf{S}^{+}\mathbf{U}\mathbf{U}^{+}\mathbf{S}\}_{\mathrm{diag}}$, is now formed applying the adjoint operator $\mathbf{S}^{+}$, and the windowing of the rough SS $\mathbf{\Pi}$ is performed applying the smoothing filter $\mathbf{\Omega} = (w_0\mathbf{I} + \mathbf{M})^{-1}$ with the nonnegative entry, the same one as was constructed numerically by Shkvarko (2004a, 2004b). Equation (26) can be referred to as *Matched Filtering* (MF) algorithms for estimation of the SSP and RSS, respectively. This definition will become apparent from the following explanation. Observe, that equation (26) is recognised to be a vector-form representation of the conventional kernel SSP estimation algorithm (Henderson and Lewis, 1998), in which the SS is formed as the squared modulus of the outcomes of the matched spatial filter applied to the recorded data signal

(trajectory signal in the SAR terminology (Henderson and Lewis, 1998; Mahafza, 2000)). Thus, in the framework of the FBR inference-based approach to RS imaging (Shkvarko, 2002a, 2002b), the traditional MF technique (26a) can be viewed as a rough simplified version of the derived above RRF algorithm (24) with its corresponding generalisation (26) for the case of the RSS estimator. In view of this, in the presented family of the SSP and RSS estimators, we specify equation (26) as the rough MF method for SSP and RSS estimation, whereas we refer to (24) as the suboptimal Robust Reconstructive Filtering (RRF) enhanced imaging method, and, finally, we refer to equations (16) and (21) as the complete FBR-optimal or Adaptive Reconstructive Filtering (ARF) techniques for numerical reconstruction of the SSP and RSS, respectively.

5 ARRMENN method

5.1 NN-based computing scheme

In this Section, we propose the NN-based computing scheme for efficient real-time implementation of the above presented RRF method. The main idea is to aggregate the robust regularisation with the NN-based computing to reduce the computational load of the RRF method. We approach this goal by performing the modifications of the multistate Hopfield-type modified maximum entropy NN (MENN) originally developed by Shkvarko et al. (2001). The modification that we perform is aimed at enabling such the NN to implement computationally the RRF algorithm (24). Borrowing from the work of Shkvarko et al. (2001) we define the Hopfield-type NN as a massive interconnection of formal neurons, i.e., basic processing units. The outputs of all K neurons compose the output vector, $\mathbf{z} = \mathrm{sgn}(\mathbf{Q}\mathbf{v} + \mathbf{\Theta})$, where, $\mathbf{Q}$ represents the $K \times K$ matrix of the interconnection strengths of the NN, and $\mathbf{\Theta}$ defines the K-d bias vector of the NN (Shkvarko et al., 2001). The output vector $\mathbf{z}$ is used to update the state vector $\mathbf{v}$ of the network: $\mathbf{v}'' = \mathbf{v}' + \Delta\mathbf{v}$ where, $\Delta\mathbf{v} = \Re(\mathbf{z})$ represents a change of the state vector v computed applying the state update rule $\Re(\mathbf{z})$, the same one as was originally designed by Shkvarko et al. (2001), where the superscripts $''$ and $'$ correspond to the state values before and after network state updating, respectively. The state update rule $\Re(\mathbf{z})$ is designed in a way (Doerry et al., 2002) that the energy function of the NN

$$E_{NN}(\mathbf{v}) = -\frac{1}{2}\mathbf{v}^{\mathrm{T}}\mathbf{Q}\mathbf{v} - \mathbf{\Theta}^{\mathrm{T}}\mathbf{v} \to \min_{\mathbf{v}} \tag{27}$$

is decreased at each updating step, i.e., $E_{NN}(\mathbf{v}'') \le E_{NN}(\mathbf{v}')$, until the NN reaches its stationary state (saddle point) related to the state $\mathbf{v}_{opt}$ at which the minimum of the NN energy is attained, i.e., $E_{NN}(\mathbf{v}_{opt}) = \min_{\mathbf{v}} E_{\mathrm{NN}}(\mathbf{v})$.

Analysing now the behaviour of such the NN we may associate the NN's stationary state with the solution to the hypothetical Inverse Problem (IP) of minimisation of the composite cost function

$$E_{IP}(\mathbf{Y} \mid \boldsymbol{\lambda}) = \frac{1}{2}\lambda_1 \,||\, \mathbf{U} - \mathbf{S}\mathbf{Y} \,||^2 + \frac{1}{2}\lambda_2 \,||\, \mathbf{Y} \,||^2 . \tag{28}$$

5.2 MENN computing for implementing the ARRMENN

Following the theory developed by Shkvarko et al. (2001), we adjust the regularisation parameters in equation (28) as, $\lambda_1 = 1$, $\lambda_2 = \rho^{-1}$, in which case the NN's stationary state is associated with the Maximum Entropy (ME) solution to equation (27) (Shkvarko, 2002a, 2002b), thus the minimisation of $E_{IP}(\mathbf{Y}|\boldsymbol{\lambda})$ provides the robust regularised constraint least square estimate $\mathbf{Y} = \mathbf{F}\mathbf{U}$ that uniquely defines the desired high-resolution SSP vector $\mathbf{V} = \{\mathbf{Y}\mathbf{Y}^{+}\}_{diag}$. Hence, the cumbersome operator inversions needed to compute the SS formation operator (22) are now translated into the problem of recurrent minimisation of the energy function (27) of such modified MENN and derivation of $\mathbf{Y} = \mathbf{v}_{opt}$ via specification of the MENN's parameters as follows

$$\mathbf{Q}_{ki} = -\lambda_1 \sum_{j=1}^{K} S_{jk} S_{ji}^{*} - \lambda_2 \delta_{ki} \ \text{ for all } \ k, i = 1, \ldots, K \tag{29}$$

and

$$\mathbf{\Theta}_k = \lambda_1 \sum_{j=1}^{K} S_{jk} U_j \quad \text{for all } k = 1, \ldots, K, \tag{30}$$

where $\mathbf{Q}_{ki}$ and $\mathbf{\Theta}_k$ represent the elements of the interconnection strengths matrix $\mathbf{Q}$ and bias vector $\mathbf{\Theta}$ of the modified MENN, respectively. Observe that because of the exclusion of the solution-dependent operator inversions (17), (22) via translations (28) of the SS formation procedure into the relevant recurrent problem of minimisation of the MENN's energy function (27) associated with the relevant E_{IP} $(\mathbf{Y}|\boldsymbol{\lambda})$ (28) the computational load of the resulting ARRMENN procedure (27), (28) is drastically decreased in comparison with the fully optimal FBR algorithm (16).

In the simulation applications (reported in the subsequent Section) related to reconstruction of the 1024-by-1024-pixel format 256-scaled environmental images, the computation load of the RS enhanced imaging with the ARRMENN algorithm (27), (28) that incorporates the proposed above MENN computational scheme in comparison with the original FBR method (16) was decreased approximately 10^5 times and required 0.38 sec of the overall computational time (i.e., real-time mode) for implementing the ARMENN technique (26)–(28) with the SONY© VAIO©VGN-A190 PC.

6 Towards dynamical computing for RSS reconstruction

6.1 RSS linear dynamic model

The crucial issue in application of the modern dynamic filter theory (Falkovich et al., 1989; Villalon-Turrubiates, 2006)

to the problem of reconstruction of the desired RSS in evolution time is related to modelling of the RSS as a random field (i.e., spatial map developing in time t) that satisfies some dynamical state equation. Following the typical linear assumptions for development of the RSS in time (Falkovich et al., 1989; Villalon-Turrubiates, 2006), we represent its dynamical model in a vectorised space-time form defined via the following stochastic differential state equation of the first order

$$\frac{d\mathbf{z}(t)}{dt} = \mathbf{F}\mathbf{z}(t) + \mathbf{G}\boldsymbol{\xi}(t), \quad \boldsymbol{\Lambda}(t) = \mathbf{C}\mathbf{z}(t) \tag{31}$$

where $\mathbf{z}(t)$ is the so-called model *state vector*; $\mathbf{C}$ defines a linear operator that introduces the relation between the RSS and the state vector $\mathbf{z}(t)$, and $\boldsymbol{\xi}(t)$ represents the white model generation noise vector characterised by the statistics, $\langle \boldsymbol{\xi}(t) \rangle = \mathbf{0}$ and $\langle \boldsymbol{\xi}(t)\boldsymbol{\xi}^T(t') \rangle = \mathbf{P}_{\xi}(t)\delta(t - t')$ (Falkovich et al., 1989). Here, $\mathbf{P}_{\xi}(t)$ is referred to as state model disperse matrix (Falkovich et al., 1989) that characterises the dynamics of the state variances developed in a continuous time t ($t_0 \to t$) starting from the initial instant t_0. Next, the dynamic model equation that states the relation between the time-dependent SSP (actual scene image) $\mathbf{B}(t)$ and the desired RSS map $\boldsymbol{\Lambda}(t)$ can be represented in the following form (Falkovich et al., 1989)

$$\begin{aligned} &\hat{\mathbf{B}}(t) = \mathbf{L}\mathbf{C}(t)\mathbf{z}(t) + \boldsymbol{v}(t) = \mathbf{H}(t)\mathbf{z}(t) + \boldsymbol{v}(t); \\ &\mathbf{H}(t) = \mathbf{L}\mathbf{C}(t). \end{aligned} \tag{32}$$

Here, we introduced the linearised approximation $\mathbf{L}$ (i.e., first order matrix-form approximation (Villalon-Turrubiates, 2006)) to the inverse of the RSS operator $\boldsymbol{\Lambda}(\hat{\mathbf{B}}(\mathbf{r}))$ and generalised (32) for the case of dynamical (i.e., time-dependent) RSS and SSP models. The stochastic differential model (31), (32) allows now to apply the theory of dynamical filters (Falkovich et al., 1989; Villalon-Turrubiates, 2006) to reconstruct the desired RRS in current time incorporating the a priori model dynamical information about the RSS. The aim of the dynamic filtration is to find an optimal estimate of the desired RSS, $\hat{\boldsymbol{\Lambda}}(t) = \mathbf{C}\hat{\mathbf{z}}(t)$, developed in current time, t ($t_0 \to t$), via processing the reconstructed image vector $\hat{\mathbf{B}}(t)$ (i.e., the reconstructed SSP developed in time) taking into considerations the a-priori dynamic model of the desired RSS specified through the state equation (31). In other words, one has to design an optimal dynamic filter that when applied to the reconstructed image $\hat{\mathbf{B}}(t)$ (specified by the dynamic image model (32)) provides the optimal estimation of the desired RSS map $\hat{\boldsymbol{\Lambda}}(t) = \mathbf{C}\hat{\mathbf{z}}(t)$, in which the state vector estimate $\hat{\mathbf{z}}(t)$ satisfies the a-priori dynamic behaviour modelled by the stochastic dynamic state equation (31). The canonical discrete-time solution to equation (31) in state variablesis (Villalon-Turrubiates, 2006)

$$\begin{aligned} &\mathbf{z}(i+1) = \boldsymbol{\Phi}(i)\mathbf{z}(i) + \boldsymbol{\Gamma}(i)\boldsymbol{\xi}(i) \\ &\boldsymbol{\Lambda}(i) = \mathbf{C}(i)\mathbf{z}(i); \end{aligned} \tag{33}$$

where $\boldsymbol{\Phi}(i) = \mathbf{F}(t_i)\Delta t + \mathbf{I}$; $\boldsymbol{\Gamma}(i) = \mathbf{G}(t_i)\Delta t$, and Δt represents the time sampling interval for dynamical modelling of the RSS in discrete time. Next, we specify the statistical characteristics of the a-priori information in such a discrete time scale (Falkovich et al., 1989). These are as follows:

- generating noise model
  $\{\boldsymbol{\xi}(i)\} : \langle \boldsymbol{\xi}(i) \rangle = 0; \langle \boldsymbol{\xi}(i)\boldsymbol{\xi}^{\mathrm{T}}(j) \rangle = \mathbf{P}_{\xi}(i, j)$
- data noise $\{\nu(i)\} : \langle \nu(k) \rangle = \mathbf{0}$;
  $\langle \boldsymbol{v}(i)\boldsymbol{v}^{\mathrm{T}}(j) \rangle = \mathbf{P}_{v}(i, j);$ (34)
- state vector
  $\{\mathbf{z}(k)\} : \langle \mathbf{z}(0) \rangle = \mathbf{m}_z(0); \langle \mathbf{z}(0)\mathbf{z}^T(0) \rangle = \mathbf{P}_{\mathbf{z}}(0)$

where 0 argument implies the initial state for initial time instant, $i = 0$. For such model conventions, the disperse matrix $\mathbf{P}_z(0)$ satisfies the following *disperse* dynamic equation (Villalon-Turrubiates, 2006)

$$\begin{aligned} \mathbf{P}_z(i+1) &= \langle \mathbf{z}(i+1)\mathbf{z}^{\mathrm{T}}(i+1) \rangle \\ &= \boldsymbol{\Phi}(i)P_{\mathbf{z}}(i)\boldsymbol{\Phi}^{\mathrm{T}}(i) + \boldsymbol{\Gamma}(i)\mathbf{P}_{\xi}(i)\boldsymbol{\Gamma}^{\mathrm{T}}(i). \end{aligned} \tag{35}$$

6.2 Dynamic RSS reconstruction

The problem now is to design an optimal decision procedure (optimal filter) that, when applied to all reconstructed images $\{\hat{\mathbf{B}}(i)\}$ (ordered in a discrete time i, ($i_0 \to i$)), provides an optimal solution to the desired RSS represented via the estimate of the state vector state vector $\mathbf{z}(i)$ subject to the numerical dynamic model (33). To proceed with derivation of such a filter, we first represent the state equation (31) in discrete time i, ($i_0 \to i$):

$$\mathbf{z}(i+1) = \boldsymbol{\Phi}(i)\mathbf{z}(i) + \boldsymbol{\Gamma}(i)\boldsymbol{\xi}(i). \tag{36}$$

Next, according to this dynamical model, the anticipated mean value for the state vector can be expressed as

$$\mathbf{m}_z(i+1) = \langle \mathbf{z}(i+1) \rangle = \langle \mathbf{z}(i+1) \mid \hat{\mathbf{z}}(i) \rangle. \tag{37}$$

The $\mathbf{m}_z(i+1)$ is considered as the a-priori conditional mean value of the state vector for the $(i+1)$st estimation step, thus from equations (36), (37) we obtain

$$\begin{aligned} \mathbf{m}_z(i+1) &= \boldsymbol{\Phi}\langle \mathbf{z}(i) \mid \hat{\mathbf{B}}(0), \hat{\mathbf{B}}(1), \ldots, \hat{\mathbf{B}}(i) \rangle + \boldsymbol{\Gamma}\langle \boldsymbol{\xi}(i) \rangle \\ &= \boldsymbol{\Phi}\hat{\mathbf{z}}(i). \end{aligned} \tag{38}$$

and the prognosis of the mean value becomes, $\mathbf{m}_z(i+1) = \boldsymbol{\Phi}\hat{\mathbf{z}}(i)$. From equations (36) – (38) one may deduce that given the fact that the particular reconstructed

image $\hat{\mathbf{B}}(i)$ is treated at discrete time i, it makes the previous reconstructions $\{\hat{\mathbf{B}}(0),\hat{\mathbf{B}}(1),\dots\hat{\mathbf{B}}(i-1)\}$ irrelevant, hence the optimal filtering strategy is reduced to the dynamical one-step predictor. Thus, using these derivations, we next modify the dynamical estimation strategy to such one-step optimal prediction procedure as follows,

$$\begin{aligned}\hat{\mathbf{z}}(\mathrm{i}+1)&=\langle \mathbf{z}(i+1)\mid \hat{\mathbf{B}}(0),\hat{\mathbf{B}}(1),\dots,\hat{\mathbf{B}}(i),\hat{\mathbf{B}}(i+1)\rangle\\ &=\langle \mathbf{z}(i+1)\mid \hat{\mathbf{z}}(i);\hat{\mathbf{B}}(i+1)\rangle\\ &=\langle \mathbf{z}(i+1)\mid \hat{\mathbf{B}}(i+1);\mathbf{m}_z(i+1)\rangle.\end{aligned} \tag{39}$$

Hence, for the current $(i+1)$-st discrete-time prediction-estimation step, the dynamical RSS estimate (32) becomes

$$\hat{\mathbf{B}}(i+1)=\mathbf{H}(i+1)\mathbf{z}(i+1)+\boldsymbol{v}(i+1) \tag{40}$$

with the a-priori predicted mean (37) for the desired state vector. Applying now the Wiener minimum risk strategy (Villalon-Turrubiates, 2006) to solve equations (40) with respect to the state vector $\mathbf{z}(t)$ and taking into account the a priori information summarised by equation (34), we obtain the dynamic solution for the RSS state vector

$$\begin{aligned}\hat{\mathbf{z}}(i+1)&=\mathbf{m}_{\mathbf{z}}(i+1)+\boldsymbol{\Sigma}(i+1)[\hat{\mathbf{B}}(i+1)\\ &\quad-\mathbf{H}(i+1)\mathbf{m}_{\mathbf{z}}(i+1)]\end{aligned} \tag{41}$$

where the desired dynamic filter operator $\boldsymbol{\Sigma}(i+1)$ is defined as follows,

$$\begin{aligned}&\boldsymbol{\Sigma}(i+1)=\mathbf{K}_{\boldsymbol{\Sigma}}(i+1)\mathbf{H}^{\mathrm{T}}(i+1)\mathbf{P}_v^{-1}(i+1);\\ &\mathbf{K}_{\boldsymbol{\Sigma}}(i+1)=\left[\boldsymbol{\Psi}_{\boldsymbol{\Sigma}}(i+1)+\mathbf{P}_{\mathbf{z}}^{-1}(i+1)\right]^{-1};\\ &\boldsymbol{\Psi}_{\boldsymbol{\Sigma}}(i+1)=\mathbf{H}^{\mathrm{T}}(i+1)\mathbf{P}_v^{-1}(i+1)\mathbf{H}(i+1).\end{aligned} \tag{42}$$

Last, using the derived filter equations (41), (42) and the initial RSS state model given by equation (33), we finally obtain the optimal filtering procedure for dynamic reconstruction of the desired RSS map in the current discrete time $i=0,1,\dots$

$$\begin{aligned}\hat{\boldsymbol{\Lambda}}(i+1)&=\boldsymbol{\Phi}(i)\hat{\mathbf{z}}(i)+\boldsymbol{\Sigma}(i+1)[\hat{\mathbf{B}}(i+1)\\ &\quad-\mathbf{H}(i+1)\boldsymbol{\Phi}(i)\hat{\mathbf{z}}(i)];\quad i=0,1,\dots\end{aligned} \tag{43}$$

with the initial condition, $\hat{\boldsymbol{\Lambda}}(0)=\boldsymbol{\Lambda}\{\hat{\mathbf{B}}(0)\}$, and a priori statistics specified by equation (34). Figure 1 shows the information flow diagram that illustrates the overall fused procedure for RSS reconstruction and dynamic filtration. As a primary part, the SSP image reconstruction is to be performed. Next, the desired particular RSS map is to be reconstructed in a dynamic fashion. All necessary algorithmic details for computational implementation of such fused dynamical SSP-RSS reconstruction were explicitly specified in this section and in two previous sections. The crucial issue to note here is related to model uncertainties regarding the particular employed dynamical RSS model (33), hence the corresponding uncertainties regarding the overall dynamically reconstructed RSS. These issues require more investigations and are the matter of further studies.

7 Computer simulation experiment

7.1 Simulation experiment specifications

We simulated a conventional side-looking SAR as particular sensor system with the fractionally synthesised aperture i.e., the array was synthesised by the moving antenna. The SFO of such a SAR is factored along two axes in the image plane (Shkvarko, 2004a, 2004b): the azimuth (horizontal axis, x_1) and the range (vertical axis, x_2). In the simulations, we considered the conventional triangular SAR range Ambiguity Function (AF) $\Psi_r(x_2)$ and Gaussian approximation, i.e., $\Psi_r(x_1)=\exp(-(x_1)^2/a^2)$, of the SAR azimuth AF with the adjustable fractional parameter a (Shkvarko, 2004a, 2004b). Note that in the RS imaging the AF is referred to as the continuous-form approximation of the ambiguity operator matrix $\boldsymbol{\Psi}=\mathbf{S}^{+}\mathbf{S}$ and serves as an equivalent to the point spread function in the conventional image processing terminology (Kang and Katsaggelos, 1995; Starck et al., 1998). In this paper, we present the simulations performed with the real-world 256-scaled RS images of 1024-by-1024-pixel format (south-west Guadalajara region, Mexico (Shkvarko and Villalon-Turrubiates, 2005). In the reported simulations, the resolution cell along the x_2 direction was adjusted to the effective width of the range AF for the both simulated scenarios. In the x_1 direction, the fractional parameter a was controlled to adjust different effective widths $\Delta\boldsymbol{\Psi}_a(x_1)$ of the azimuth AF.

7.2 Quality metric

For the purpose of objectively testing the performances of different ARRMENN related SSP and RSS estimation algorithms, a quantitative evaluation of the improvement in the estimates (gained due to applying the suboptimal and optimal IFOs $\mathbf{F}^{(1)}$ and $\mathbf{F}^{(3)}$ instead of the adjoint operator $\mathbf{F}^{(2)}=\mathbf{S}^{+}$) was accomplished. In analogy to image reconstruction (Puetter, 1996; Shkvarko, 2004a, 2004b), we use the quality metric defined as an improvement. In the Output Signal-to-Noise Ratio (IOSNR)

$$IOSNR^{(RRF)}=10.\log_{10}\cdot\frac{\sum_{k=1}^{K}(\hat{B}_k^{(MF)}-B_k)^2}{\sum_{k=1}^{K}(\hat{B}_k^{(RRF)}-B_k)^2}; \tag{44}$$

$$IOSNR^{(ARF)}=10.\log_{10}\cdot\frac{\sum_{k=1}^{K}(\hat{B}_k^{(MF)}-B_k)^2}{\sum_{k=1}^{K}(\hat{B}_k^{(ASF)}-B_k)^2} \tag{45}$$

where B_k represents a value of the kth element (pixel) of the original SSP B, $\hat{B}_k^{MF}$ represents a pixel value of the kth element (pixel) of the rough SSP estimate $\hat{B}_{MF}$, $\hat{B}_k^{(RRF)}$ represents a value of the kth pixel of the suboptimal SSP estimate $\hat{B}_{RRF}$, and $\hat{B}_k^{(ARF)}$ corresponds to the kth pixel

value of the SDR-optimised SSP ARF , respectively. $IOSNR^{(RRF)}$ corresponds to the RRF estimator and $IOSNR^{(ARF)}$ corresponds to the ARF method. According to (44), the higher the IOSNR, the better the improvement in the SSP estimate is, i.e., the closer the estimate is to the original SSP.

Figure 1 Block diagrams of the image and RSS reconstruction and dynamical post-processing techniques

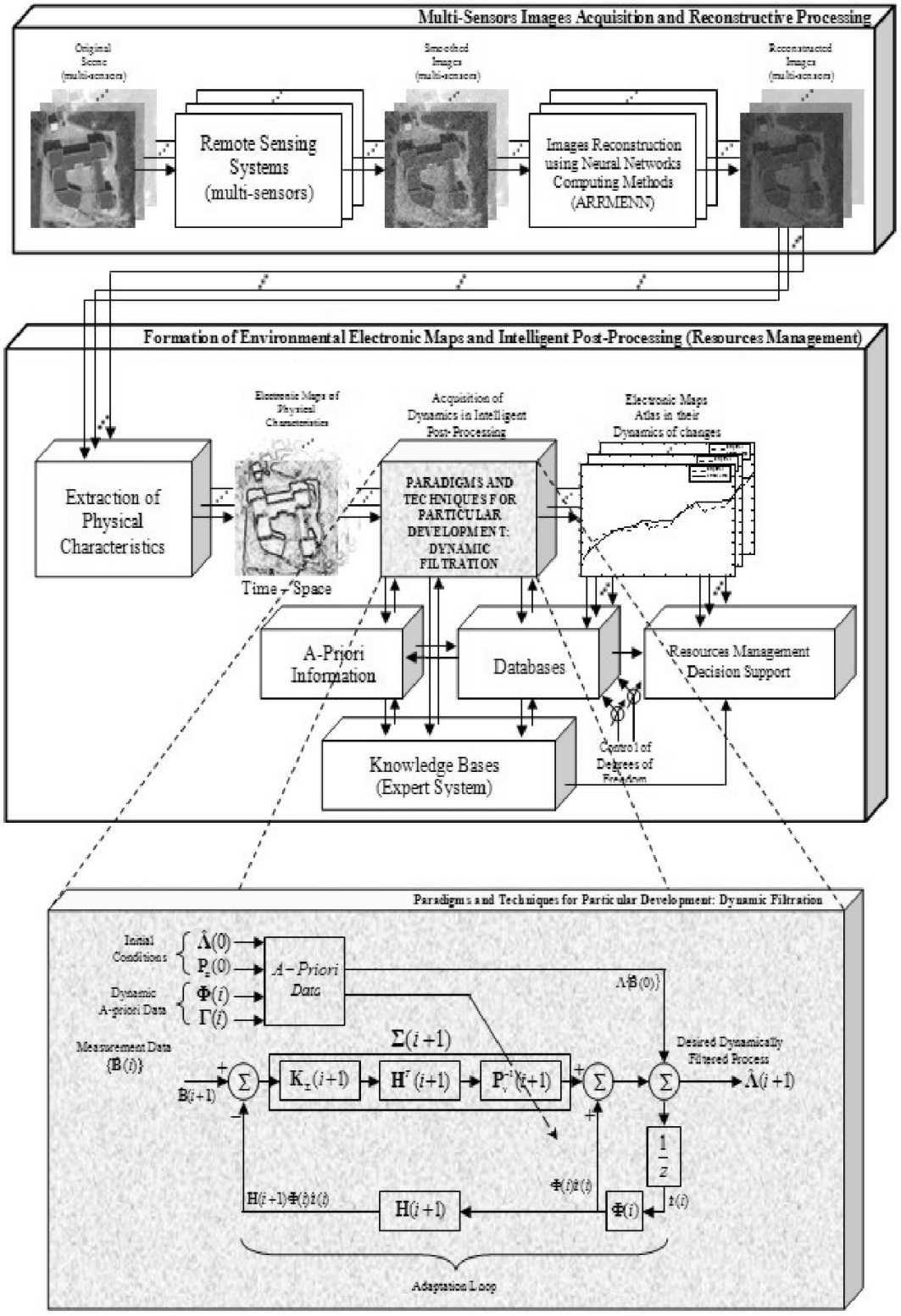

7.3 Simulation results with image reconstruction

Figure 2(a) shows the high-resolution image of the original scene borrowed from the RS imagery provided with the super-resolution SAR (Shkvarko and Villalon- Turrubiates, 2005). The simulations of conventional-resolution (i.e., fractionally synthesised) SAR imaging and computer-aided image enhancement that employ the IFOs given by (26), (22) and (17) are displayed in Figures 2(b)–(d), respectively. The enhanced images presented in Figures 2(c) and (d) were numerically reconstructed from the rough image of Figure 2(b) for the case of white Gaussian observation noise with the Signal-to-Noise Ratio (SNR) $\mu = 20$ dB and the fractional parameter a adjusted to provide the horizontal width $\Delta\Psi_a(x_1)$ of the discretised azimuth AF $\Delta\Psi_a(x_1)$ at a half of its peak level equal to 16 pixels. Figure 3 shows the extraction of physical characteristics using the RSS linear dynamic model. In Table 1, we report the IOSNRs (in the dB scale) gained with the derived above RRF and ARF enhanced imaging algorithms for typical SAR system models that operate under different SNRs levels μ for two typical operation scenarios with different widths of the fractionally synthesised apertures: $\Delta\Psi_a(x_1) = 16$ pixels (first system) and $\Delta\Psi_a(x_1) = 32$ pixels (second system). The higher values of $IOSNR^{(RRF)}$ as well as $IOSNR^{(ARF)}$ were obtained in the second scenario. Note that *IOSNR* (31) is basically a squire-type error metric. Thus, it does not qualify quantitatively the 'delicate' visual features in the images, hence, small differences in the corresponding *IOSNRs* reported in Table 1. In addition, both enhanced estimators manifest the higher *IOSNRs* in the case of more smooth azimuth AFs (larger values of . $\Delta\Psi_a(x_1)$) and higher SNRs μ. The advantage of the ARRMENN reconstructed images (cases $\hat{\mathbf{B}}_{RRF}$ and $\hat{\mathbf{B}}_{ARF}$) over the conventional case $\hat{\mathbf{B}}_{MF}$ is evident. Due to the performed regularised SFO inversions the resolution was improved in the both cases, $\hat{\mathbf{B}}_{RRF}$ and $\hat{\mathbf{B}}_{ARF}$, respectively.

For the ARRMENN-optimised reconstructed SSP, $\hat{\mathbf{B}}_{ARF}$, in addition, the ringing effects were reduced, while the RRF robustified estimator with the IFO given by equation (22) did not require adaptive iterative computing, thus resulted in the processing with substantial reduced computational load (e.g., in the reported simulations, the RRF algorithm required approximately 40 times less computations than the ARF (17) computationally implemented with the ARRMENN algorithm (26)). These results qualitatively demonstrate that with some proper adjustment of the degrees of freedom in the general FBR-optimised estimator (16), one could approach the quality of the optimal FBR reconstructive imaging method avoiding the cumbersome adaptive computations. Such an optimisation is a matter of the further studies.

7.4 Simulation results with RSS dynamical filtration

In Figures 3(a)–(e), we present some simulation results of dynamic reconstruction-filtration of a particular RSS that represents the so-called *Integral Hydrological Index* (IHI) map extracted from the reconstructed images $\{\hat{\mathbf{B}}\}$.

Figure 2 Simulation results of SSP reconstruction of the SAR data: (a) original super-high resolution scene image (not observed in the imaging experiment); (b) low-resolution scene image formed applying the MF method; (c) scene image enhanced with the RRF method computationally implemented with the ARMENN algorithm and (d) the same scene image optimally enhanced applying the ARF method computationally implemented with the ARMENN algorithm

(a)

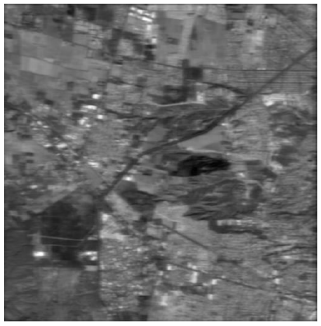

(b)

(c)

(d)

Figure 3 Simulation results of post-processing and dynamical filtration of the RSS using SAR data: (a) integral hydrological index (IHI) map extracted from the low-resolution image 2(b); (b) dynamics for a particular zone of the IHI map extracted from image 3(a); (c) IHI map extracted from the reconstructed image 2(c); (d) dynamics for the same particular zone of the IHI map extracted from image 3(c); (e) IHI map extracted from the reconstructed image 2(d) and (f) dynamics for the same particular zone of the IHI map extracted from image 3(e)

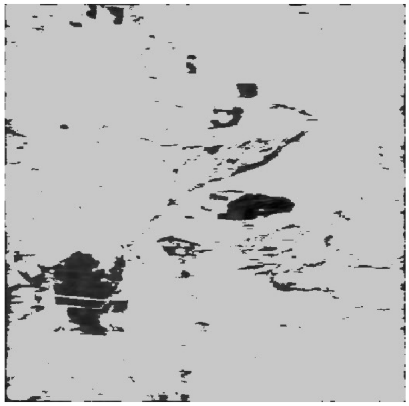

(a)

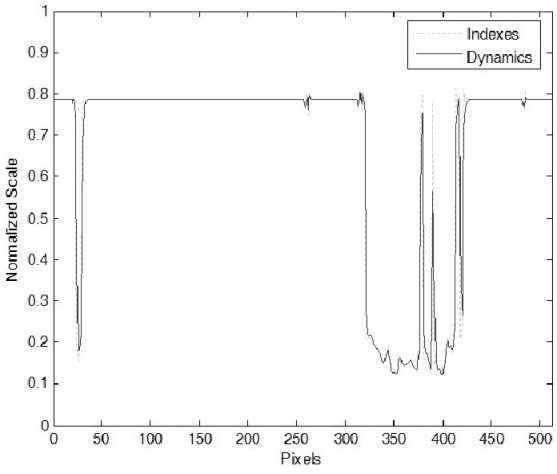

(b)

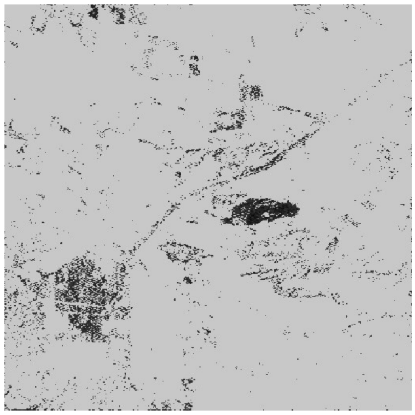

(c)

Figure 3 Simulation results of post-processing and dynamical filtration of the RSS using SAR data: (a) integral hydrological index (IHI) map extracted from the low-resolution image 2(b); (b) dynamics for a particular zone of the IHI map extracted from image 3(a); (c) IHI map extracted from the reconstructed image 2(c); (d) dynamics for the same particular zone of the IHI map extracted from image 3(c); (e) IHI map extracted from the reconstructed image 2(d) and (f) dynamics for the same particular zone of the IHI map extracted from image 3(e) (continued)

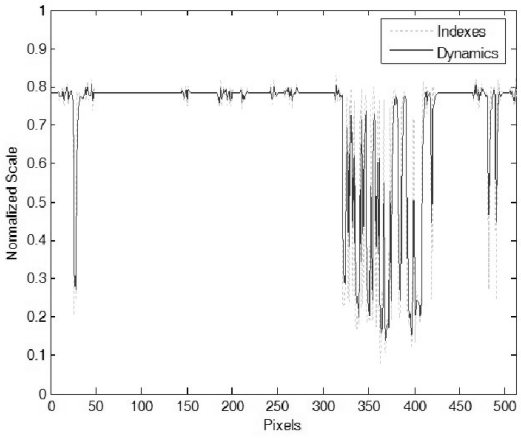

(d)

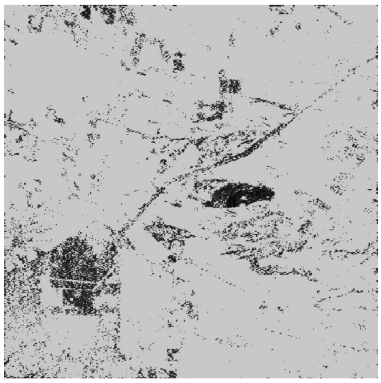

(e)

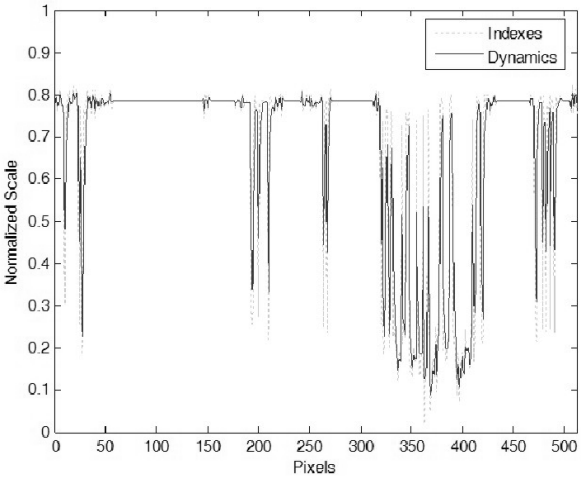

(f)

Table 1 IOSNR values provided with the two simulated methods: RRF and ARF results are reported for two SAR system models with different resolution parameters and different SNRs

SNR, μ (dB)	*First system*, $\Delta\Psi$ = 16 (dB)		*Second system*, $\Delta\Psi_a$ = 32 (dB)	
	$IOSNR^{(RRF)}$	$IOSNR^{(ARF)}$	$IOSNR^{(RRF)}$	$IOSNR^{(ARF)}$
15	2.24	3.20	2.62	3.89
20	3.34	4.32	4.47	5.78
25	4.20	5.12	5.31	7.42
30	5.55	6.24	6.45	9.19

The particular reported simulations are specified in the figure captures. The IHI map is extracted from the original brightness reconstructed image applying the truncated (two-edge) histogram filter operator with the empirically adjusted lower threshold th_L and upper threshold th_U. Within the truncation interval ($th_U - th_L$), the IHI extraction operator provides homogeneous translation (Henderson and Lewis, 1998) of the scaled reconstructed images $\{\hat{\mathbf{B}}\}$ in to the RSS map $\{\hat{\mathbf{\Lambda}}\}$.

In the particular reported here simulations, based on the previously gained experience by Villalon-Turrubiates (2006), the thresholds were adjusted as follows, $th_L = 60$ pixels and $th_U = 200$ pixels of the 256 pixel scale of greys. Following Henderson and Lewis (1998), the 'mirror reflected' inverse truncated histogram filter was used as an approximation to the RSS extraction operator $\mathbf{L}$ in the dynamic model of the RSS reconstruction filter specified in Section 6.

As the purpose of the experimental study was to investigate the possibility to perform the dynamic RSS filtering in the realistic conditions of minimum prior model knowledge regarding the dynamical behaviour of the particular RSS, the dynamic IHI information was robustified to the simplest maximum entropy model (Henderson and Lewis, 1998) of the transfer matrix $\mathbf{\Phi}(i) = \mathbf{I}$ with initialising assumptions, $\mathbf{P}_{\nu}(0) = \mathbf{I}, \mathbf{P}_{\mathbf{z}}(0) = \mathbf{I}$.

The dynamical reconstructions were performed iteratively applying the algorithm (43) to the images reconstructed with three different algorithms, MF, RRF and ARRMENN, respectively. These served as particular input data for algorithm (43), i.e.,

$$\hat{\mathbf{\Lambda}}^{(1)}(0) = \Lambda\{\hat{\mathbf{B}}^{(1)}(0) = \hat{\mathbf{B}}_{MF}\},$$

$$\hat{\mathbf{\Lambda}}^{(2)}(0) = \Lambda\{\hat{\mathbf{B}}^{(2)}(0) = \hat{\mathbf{B}}_{RRF}\}, \text{ and}$$

$$\hat{\mathbf{\Lambda}}^{(3)}(0) = \Lambda\{\hat{\mathbf{B}}^{(3)}(0) = \hat{\mathbf{B}}_{ARF}\}, \text{ respectively.}$$

Also, in Figure 3(b–d) and (f), we present the simulation results of the dynamics for the IHI maps extracted from the MF, RRF and ARF reconstructed images, respectively. The reported optimally filtered IHIs are indicative of the dynamical behaviour of the RSS. The RSS filtered from the previously enhanced images using the dynamical filter fused with the ARRMENN reconstruction related to the $\hat{\mathbf{B}}_{RRF}$ and $\hat{\mathbf{B}}_{ARF}$ over the RSS dynamics extracted from the rough images ($\hat{\mathbf{B}}_{MF}$) is evident. The IHI map and the indexes dynamics are much more detailed in both cases.

Also, the dynamical reconstructions performed iteratively applying the algorithm (43) resulted in the processing with substantial reduced computational load. The reported results qualitatively demonstrate that with proper adjustment of the degrees of freedom in the general algorithm (43), one could predict the dynamic behaviour of the IHI maps. The detailed investigation of the prediction methodology is a matter of the further studies.

8 Conclusion and perspectives

In this paper, we have presented the aggregated robust regularised maximum entropy neural network (ARRMENN) approach for solving the nonlinear inverse problems of high-resolution reconstruction of the SSP and RSS of the remotely sensed scenes via processing the finite-dimensional space-time measurements of the available sensor system signals as it is required, for example, for enhanced RS imaging/scene mapping with imaging radar/SAR.

Our study revealed some new aspects of designing the optimal/suboptimal SSP and RSS estimators and numerical imaging techniques important both for the theory and practical implementation.

To derive the optimal numerical SSP and RSS estimators, we proposed the fused ARRMENN strategy that incorporated the non-trivial a priori information on the desired image signatures through unifying the regularisation considerations with the minimum risk statistical estimation paradigm. Being nonlinear and solution dependent, the general optimal solution-dependent SSP and RSS estimators require adaptive signal processing operations that result in a very cumbersome computing. The computational complexity arises due to the necessity to perform simultaneously the solution-dependent operator inversions with control of the regularisation degrees of freedom.

However, we have proposed a robustified approach for some simplifications of the general optimal Adaptive Reconstructive Filtering (ARF) estimator that leads to the computationally efficient Robust Reconstructive Filtering (RRF) method. In the terms of regularisation theory, the RRF method may be interpreted as robustified image/signature enhancement/reconstruction technique. Indeed, with an adequate selection of some design parameters that contain the RRF and ARF estimators, the reconstructed scene image performances can be substantially improved if compared with those obtained using the conventional MF method that is traditionally implemented in all existing remote sensing and imaging systems that employ the array imaging radars, side looking airborne radars or SAR. This was demonstrated in the simulation experiment of enhancement of the SAR images related to some typical remote sensing operational scenarios.

Also, as a matter for perspective study, we have addressed the dynamical RSS post-processing scheme that reveals some possible approach toward a new dynamic computational paradigm for high-resolution fused numerical reconstruction and filtration of different RSS maps in evolution time. In future work, we intend to develop a family of such dynamical versions of the ARRMENN-based algorithms for updating the relevant RSS maps in evolution discrete time.

Acknowledgements

We are grateful for the computing resources provided by CINVESTAV Unidad Guadalajara.

References

Astola, J. and Kuosmanen, P. (1997) *Fundamentals of Nonlinear Digital Filtering*, CRC Press, USA.

Bell, D.C. and Narayanan, R.M. (2001) 'Theoretical aspects of radar imaging using stochastic waveforms', *IEEE Transactions on Signal Processing*, Vol. 49, February, pp.394–400.

Doerry, A.W., Dickey, F.M., Romero, L.A. and DeLaurentis, J.M. (2002) 'Difficulties in superresolving SAR images', *SPIE Proceedings*, April, Vol. 4727, pp.122–133.

Falkovich, S.E., Ponomaryov, V.I. and Shkvarko, Y.V. (1989) *Optimal Reception of Space-Time Signals in Channels with Scattering*, Radio i Sviaz Press, Russia.

Haykin, S. and Steinhardt, A. (1992) *Adaptive Radar Detection and Estimation*, John Willey and Sons, USA.

Henderson, F.M. and Lewis, A.V. (1998) *Principles and Applications of Imaging Radar – Manual of Remote Sensing*, John Wiley and Sons, USA.

Kang, M.G. and Katsaggelos, A.K. (1995) 'General choice of the regularization functional in regularized image reconstruction', *IEEE Transactions on Image Processing*, Vol. 4, February, pp.594–602.

Mahafza, B.R. (2000) *Radar Systems Analysis and Design Using MATLAB*, CRC Press, USA.

Mesarovic, A., Galatsanos, N.P. and Katsaggelos, A.K. (1995) 'Regularized constrained total least squares image restoration', *IEEE Transactions on Image Processing*, Vol. 4, February, pp.1096–1108.

Puetter, R.C. (1996) 'Information, language and pixon-based image reconstruction', *SPIE Proceedings*, Vol. 2827, pp.12–31.

Shkvarko, Y.V., Shmaliy, Y.S., Jaime-Rivas, R. and Torres-Cisneros, M. (2001) 'System fusion in passive sensing using a modified Hopfield network', *Journal of the Franklin Institute*, Vol. 338, June, pp.405–427.

Shkvarko, Y.V. (2002a) 'Theoretical aspects of array radar imaging via fusing experiment design and descriptive regularization techniques', *Proceedings of the 2nd IEEE Sensor Array and Multichannel Signal Processing Workshop*, August, Washington, USA, CD-ROM.

Shkvarko, Y.V. (2002b) 'Estimation of wavefield power distribution in the remotely sensed environment: Bayesian maximum entropy approach', *IEEE Transactions on Signal Processing*, September, Vol. 50, pp.2333–2346.

Shkvarko, Y.V. (2004a) 'Unifying regularization and Bayesian estimation methods for enhanced imaging with remotely sensed data – Part I: theory', *IEEE Transactions on Geoscience and Remote Sensing*, Vol. 42, May, pp.923–931.

Shkvarko, Y.V. (2004b) 'Unifying regularization and bayesian estimation methods for enhanced imaging with remotely sensed data – part II: implementation and performance issues', *IEEE Transactions on Geoscience and Remote Sensing*, Vol. 42, May, pp.932–940.

Shkvarko, Y.V. and Villalon-Turrubiates, I.E. (2005) 'Intelligent processing of remote sensing imagery for decision support in environmental resource management: a neural computing paradigm', *Proceedings of the 2005 Information Resource Management Association International Conference*, May, San Diego, USA, CD-ROM.

Starck, J.L., Murtagh, F. and Bijaoui, A. (1998) *Image Processing and Data Analysis – The Multiscale Approach*, Cambridge University Press, UK.

Stoica, P. and Moses, R. (1997) *Introduction to Spectral Analysis*, Prentice-Hall, USA.

Villalon-Turrubiates, I.E. (2006) 'Intelligent processing for SAR imagery for environmental management', *Proceedings of the 2006 Information Resource Management Association International Conference*, May, Washington, USA, CD-ROM.